Water Resources Research

RESEARCH ARTICLE
10.1029/2019WR024905

Special Section:
Advances In Remote Sensing, Measurement, And Simulation Of Seasonal Snow

Within-Stand Boundary Effects on Snow Water Equivalent Distribution in Forested Areas

R. W. Webb[1,2,3], M. S. Raleigh[4,5], D. McGrath[6], N. P. Molotch[2,7], K. Elder[8], C. Hiemstra[9], L. Brucker[10,11], and H. P. Marshall[12,13]

[1]Department of Civil, Construction, and Environmental Engineering, University of New Mexico, Albuquerque, NM, USA, [2]Institute of Arctic and Alpine Research, University of Colorado Boulder, Boulder, CO, USA, [3]Center for Water and the Environment, University of New Mexico, Albuquerque, NM, USA, [4]Department of Geological Sciences, University of Colorado Boulder, Boulder, CO, USA, [5]National Snow and Ice Data Center, CIRES, University of Colorado Boulder, Boulder, CO, USA, [6]Department of Geosciences, Colorado State University, Fort Collins, CO, USA, [7]Department of Geography, University of Colorado Boulder, Boulder, CO, USA, [8]Rocky Mountain Research Station, USDA Forest Service, Fort Collins, CO, USA, [9]U.S. Army Corps of Engineers, Cold Regions Research and Engineering Laboratory, Fort Wainwright, AK, USA, [10]NASA Goddard Space Flight Center, Cryospheric Sciences Laboratory, Greenbelt, MD, USA, [11]Universities Space Research Association, Goddard Earth Sciences Technology and Research Studies and Investigations, Columbia, MD, USA, [12]Department of Geosciences, Boise State University, Boise, ID, USA, [13]U.S. Army Corps of Engineers, Cold Regions Research and Engineering Laboratory, Hanover, NH, USA

Abstract Forested areas exhibit high spatial variability in the distribution of snow water equivalent (SWE). Previous work has focused on forested areas with respect to snow accumulation in adjacent clearings. There is generally less snow in forested areas with greater variability relative to open areas due to the influence of tree canopies. However, the length scale of the transition from open areas to forested conditions is uncertain. Hence, the goal of this paper is to determine the length scales associated with forest boundary effects on SWE accumulation distribution patterns within forest stands. To accomplish this, we utilize a unique ground-penetrating radar data set collected during the NASA SnowEx campaign on Grand Mesa, Colorado, in February 2017 to determine spatial SWE distribution patterns of areas under canopy and in clearings, and the length scales of transitions between these patterns (i.e., the size of within-stand boundary areas). We define within-stand boundary areas as the transitional zone from a clearing to relatively stable SWE distribution, or background distribution patterns, within forest stands. The largest within-stand boundary effect occurred on the leeward side of stands with a mean extent of 44 m, or 4.3 mean canopy heights. In contrast, windward within-stand boundary effects showed a mean extent of 28 m, or 3.7 mean canopy heights. We present a conceptual framework of the complex wind dynamics that occur in forest stands to explain the within-stand boundary effects on SWE distribution. Future investigations could improve understanding of this complex process and associated driving variables.

Key Points:
- Boundary effects extend into forested areas 3.7 and 4.3 mean canopy heights on windward and leeward sides of stands, respectively
- These effects are a result of complex wind dynamics including eddies and spatially varying effective roughness near forest boundaries
- SWE variability is significantly different in forest boundary affected areas relative to background under canopy variability

Supporting Information:
- Supporting Information S1

Correspondence to:
R. W. Webb,
rwebb@unm.edu

Citation:
Webb, R. W., Raleigh, M. S., McGrath, D., Molotch, N. P., Elder, K., Hiemstra, C., et al. (2020). Within-stand boundary effects on snow water equivalent distribution in forested areas. *Water Resources Research*, *56*, e2019WR024905. https://doi.org/10.1029/2019WR024905

Received 31 JAN 2019
Accepted 29 JUN 2020
Accepted article online 4 JUL 2020

1. Introduction

Water originating from seasonal snowpacks provides vital resources for over a billion people globally (Mankin et al., 2015) and is valued at billions of dollars annually in the western United States (Sturm et al., 2017). The availability of valuable water resources from snow depends on accumulation and melt patterns, which drive diurnal and seasonal fluctuations in streamflow (Barnhart et al., 2016; Jencso & McGlynn, 2011; Lundquist & Dettinger, 2005; Mutzner et al., 2015) and hillslope-stream connectivity (McNamara et al., 2005; Webb, Fassnacht, et al., 2018). Within a watershed, snow accumulation and melt vary with elevation, topography (e.g., aspect and slope), and canopy effects on wind redistribution and energy budgets (Blöschl, 1999; Elder et al., 1991; Molotch & Meromy, 2014; Webb, 2017). Canopy effects result in higher spatial variability of snow depth and snowmelt (Andreadis et al., 2009; Lopez-Moreno & Latron, 2008; Moeser et al., 2016; Musselman, Molotch, Margulis, Kirchner, et al., 2012) that can similarly increase variability of infiltration patterns (Lundberg et al., 2016; Webb et al., 2015) enough to impact runoff processes (Webb, Williams et al., 2018). Numerous studies of snow-forest interactions have occurred (e.g., Lundquist et al., 2013; Pomeroy et al., 1998; Varhola et al., 2010). However, field and modeling studies on canopy-snow interactions have often been limited to the plot scale (e.g., Troendle & Meiman, 1986; Troendle et al., 1988) with little quantitative focus in the transitional zones across forest stand boundaries,

or the forest-meadow and forest-shrubland ecotones (e.g., Gosz, 1993). There is generally less snow and higher variability in forested areas relative to open areas due to the influence of tree canopies, with wind direction and orientation being important factors (e.g., Golding & Swanson, 1986; Wheeler, 1987). However, less is known toward the spatial scales of snow water equivalent (SWE) distribution patterns across forest and non-forest ecotones.

Improving parameterizations of forest-SWE interactions remains a challenge in process-based hydrologic model development. Such improvements are challenging given the high spatial heterogeneity in forest-SWE interactions (i.e., varying over scales ranging from 1 to 10 m) such as non-uniform snow unloading from canopies, complex distributions of sub-canopy shortwave and longwave radiation, and reduction in sub-canopy wind fields (Clark et al., 2011). Many snow models were initially developed and validated in open areas rather than in forests; hence, their performance for simulating forest processes was largely unknown until the last decade. The first comprehensive assessment of model representation of forest effects on snow was during SnowMIP2 (Rutter et al., 2009), which showed that modeling SWE in forests was more challenging than in open areas. Efforts to improve how models represent SWE distributions in forests include developing high-resolution models that use detailed canopy data (Broxton et al., 2015), adding more canopy layers (e.g., Gouttevin et al., 2015), enhancing forest structure characterization and radiation transmission (Musselman, Molotch, Margulis, Lehning, et al., 2012; Varhola & Coops, 2013), and developing canopy gap modules (Sun et al., 2018). However, spatially continuous high-resolution snow observations spanning from areas under dense canopy to large clearings are required to evaluate model enhancements and further refine forest process representations.

Numerous methods are available to remotely observe snow depth and SWE (Bair et al., 2016; Bühler et al., 2015; Dozier et al., 2016; Frei et al., 2012; Nolin, 2010; Painter et al., 2016; Schneider & Molotch, 2016; Shah et al., 2016) though these methods are often hindered in areas with dense forest canopies (Bühler et al., 2016; Hopkinson et al., 2012; Tinkham et al., 2014). For example, in a recent study airborne LiDAR surveys were unable to derive snow depth at high resolution (1 m) for 17% of all forested sites analyzed (Currier et al., 2019). Ground-based observations for forested areas include point measurements of depth and density (Elder et al., 1998; Sold et al., 2013; Sturm & Holmgren, 2018) and automated meteorological stations (e.g., snow telemetry sites in the United States in forest gaps; Serreze et al., 1999).

Ground-penetrating radar (GPR) is a mature technique that has been utilized in snow applications for decades (e.g., Ellerbruch & Boyne, 1980; Griessinger et al., 2018; Gubler & Hiller, 1984; Marshall & Koh, 2008; McGrath et al., 2015; Webb, McGrath, et al., 2018) with the primary advantage being the ability to rapidly obtain near continuous estimates of snow depth and SWE over greater spatial extents than traditional ground-based techniques. Furthermore, additional snowpack properties such as density and liquid water content can be estimated from GPR data (Bradford et al., 2009; Heilig et al., 2009; Marshall et al., 2005, 2007; Webb, Jennings, et al., 2018). For SWE estimates, GPR data are less sensitive to natural snow density variability relative to other SWE estimation methods based on depth (Raleigh & Small, 2017) since density is inversely related to radar velocity (Clair & Holbrook, 2017). Because of this relationship, errors in SWE for GPR-based estimates are approximately half of other depth-based methods (Marshall et al., 2005). Thus, GPR-based SWE estimates can be used for water budget analysis, validation of snow models and remote sensing products, and spatial pattern analyses for locations that may be difficult to otherwise observe such as under canopy in forested areas. For these reasons, GPR observations were one of the ground-based remote sensing techniques deployed during the NASA SnowEx Campaign in 2017 (SnowEx17; McGrath et al., 2019).

SnowEx is a multiyear snow observation experiment with two driving scientific questions in 2017 being: (1) what is the distribution of SWE and the snow energy balance in different canopy types, canopy densities, and terrain? and (2) what is the sensitivity and accuracy of different SWE sensing techniques in different canopy types, canopy densities, and terrain? The largest field campaign of SnowEx17 occurred at Grand Mesa (GM), Colorado, with over 100 participating scientists collecting airborne, in situ, and ground-based remotely sensed data (Brucker et al., 2017; Kim, 2018; Kim et al., 2017). This was the largest snow community airborne and field experiment in the United States since the NASA Cold Lands Process Experiments in 2002–2003. Many of the field observations occurred along pre-determined 300 m long transects designed to capture variable canopy densities and terrain.

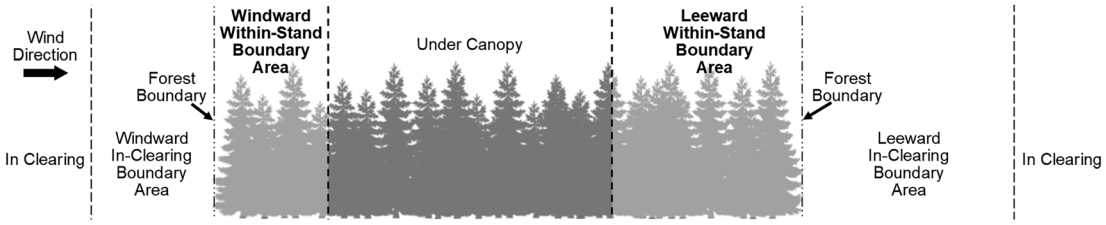

Figure 1. Defined areas as they pertain to a forest stand, its boundary, and the dominant wind direction. The within-stand boundary areas of interest for this study are labeled in bold.

Data from SnowEx17 provide opportunities to examine forest boundary effects on the SWE distribution in within-stand boundary areas. For the purposes of this paper, we define six distinct areas within and around a forest stand, defining the forest boundary as the edge between forest canopy and clearing. These areas are in clearing (present on both sides of forest stand), windward in-clearing boundary area, windward within-stand boundary area, under canopy, leeward within-stand boundary area, and leeward in-clearing boundary area (Figure 1). Previous work in canopy-snow interactions has largely focused on in-clearing boundary areas (e.g., Currier & Lundquist, 2018; Hiemstra et al., 2002, 2006) or under canopy comparisons to in clearing conditions (e.g., Lundquist et al., 2013; Varhola et al., 2010). However, there remains a gap in understanding the length scales of boundary effects on SWE distribution for within-stand boundary areas. Here we define the length scale of boundary effects as the distance from the forest boundary that the transition from in clearing to under canopy SWE distribution patterns occurs.

The goal of this paper is to quantify the length scales associated with forest boundary effects on SWE accumulation to constrain within-stand boundary areas. In other words, what distances do transitions from in-clearing boundary areas to under canopy SWE distribution patterns occur? To accomplish this, we use a GPR data set obtained during SnowEx17 on GM. We utilize this data set to assess the following research questions: (1) What are the distances from the forest boundary over which within-stand spatial patterns of SWE are affected (i.e., the extent of within-stand boundary areas in Figure 1)? and (2) Are the SWE distribution patterns significantly different in within-stand boundary areas relative to under canopy conditions?

2. Materials and Methods

2.1. Study Site Description

The GPR data collection for this study took place in February 2017 on GM in western Colorado, USA. GM has elevations ranging between 3,000 and 3,400 m.a.s.l. and is relatively flat on its western part with increasing elevation and topographic complexity from west to east. This location provides an ideal setting to investigate the influence of forest canopy on SWE distribution due to the number of isolated forest stands, or tree islands, of varying dimensions (Figure 2 and Table 1) that are dominated by Engelmann spruce (*Picea engelmannii*) and Subalpine fir (*Abies lasiocarpa*). The prevailing wind direction is from the west (Figure 3) with a seasonal snowpack that historically begins to accumulate in late October, peaks in mid-April at approximately 465 mm SWE, and melts out by late May, as measured at a nearby SNOTEL station (Mesa Lakes SNOTEL station ID 622; median values from 1981 to 2010). The SnowEx17 study period (February 2017) on GM had a mean SWE value of ~390 mm at the Mesa Lakes SNOTEL (135% of 1981–2010 median for these dates). This SNOTEL site had a peak SWE of 480 mm on 10 April with melt finishing by 1 June 2017. A similar disappearance date was also observed at a GM depth sensor array (Figure 3b; Jennings et al., 2018).

2.2. GPR Data

The GPR data presented here are a subset of a larger data set collected along 57 SnowEx transects during the first 2 weeks of the campaign (8–18 February; Webb, Jennings, et al., 2018). Transects were chosen that surveyed across forest boundaries to specifically examine within-stand boundary areas. Surveys were performed using a common-offset Mala Geosciences, Inc. ProEx GPR system, with a 1.6 GHz shielded antenna fixed in place on a plastic sled with an approximate measurement footprint of 1–2 m^2 during this study. A single-frequency GPS antenna was connected to the ProEx control unit, registering location information every second. GPR parameters evolved due to changing conditions (e.g., time window), though typical recording parameters included a waveform-sampling rate of 0.05 ns, a 40 ns time window, and “free run”

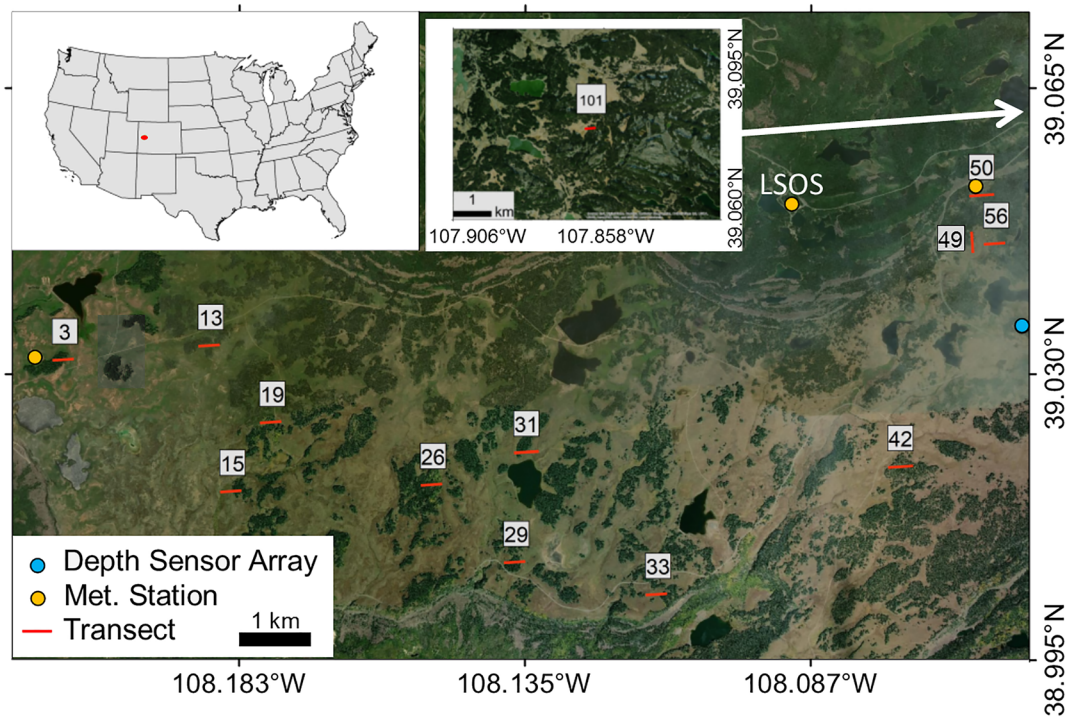

Figure 2. Overview of the Grand Mesa (GM) area of interest during the SnowEx17 field campaign showing an overview map of the transects surveyed with ground-penetrating radar and analyzed in this paper, three meteorological (met.) station locations including the local scale observation site (LSOS), and snow depth sensor array (Jennings et al., 2018). All coordinates are in decimal degrees relative to NAD83 datum (EPSG: 4269).

trace increments where samples are collected as fast as the processor allows. The system was towed behind a skier or between two snowshoers allowing data collection for all landcover types on GM, including dense forest.

Data processing was conducted using the RadExplorer software package for Week 1 of SnowEx17 and the ReflexW-2D software package for Week 2. To ensure consistency, multiple transects were processed using both programs showing similar results that were typically within 0.2 ns or ~16 mm SWE using conversion parameters described below. All radargrams were corrected to time-zero, and a dewow filter was applied. Ground surface reflection picking was done semi-automatically using manually chosen control points and a phase-following layer picker (Figure 4a).

The two-way traveltime (t) information of the ground surface reflection was then used to calculate snow depth (d_s) and estimate SWE based on density observations at snow pit locations (Ellerbruch & Boyne, 1980; Gubler & Hiller, 1984; Marshall et al., 2005). Seven snow pits (Elder et al., 2018) that were adjacent to the analyzed transects and coincidentally surveyed by the GPR were used to determine the median

Table 1
Transect Descriptors and Forest Stand Parameters Including Transect ID for SnowEx17, Orientation of the Transect That Is Either East-West (EW) or North-South (NS), Stand Length Defined as the Distance of Forest Canopy in the Direction Parallel to the Dominant Wind Direction (East-West), Stand Width Defined as the Largest Distance of Forest Canopy Along the Transect in the Direction Perpendicular to the Dominant Wind Direction (North-South), and Mean Stand Canopy Height Calculated From the September 2016 Airborne Snow Observatory LiDAR Flights (Painter, 2018)

Transect ID	3	13	15	19	26	29	31	33	42	49	50	56	101
Transect orientation	EW	EW	EW	EW	EW	EW	EW	EW	EW	NS	EW	EW	EW
Stand length (m)	230	55	275	150	605	235	135	30	70	565	620	335	540
Stand width (m)	220	130	320	800	880	360	340	220	1,310	850	635	1,390	700
Mean stand height (m)	16.1	10.3	11.0	8.3	11.9	12.0	8.5	15.2	4.7	5.8	9.2	8.5	3.9

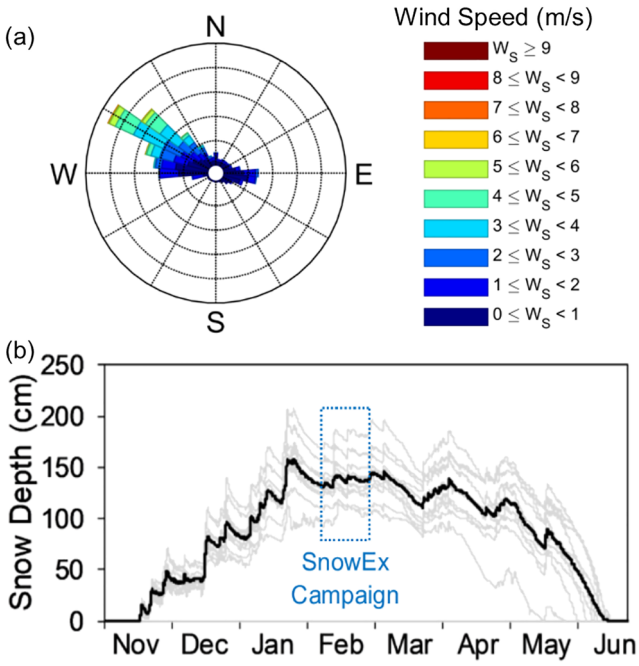

Figure 3. (a) Wind rose for the local scale observation site (LSOS) shown in Figure 2 for water year 2017 and (b) snow depth measurements from an acoustic sensor array with the solid black line representing the mean of all 10 sensors (Jennings et al., 2018).

velocity of the radar wave (v) of 0.234 m/ns (Figure 4b). Snow depth was then calculated through the following equation:

$$d_s = v * 0.5t \quad (1)$$

Depth data were converted to SWE by multiplying by the median snow density from the same seven snow pits of 335 kg/m^3 (Figure 4b). This median density is similar to the mean of all pit observed density values during SnowEx17 (Figure 4c). Uncertainty estimates for GPR-derived SWE values were estimated using the range of observed bulk densities (Figure 4) and estimated accuracy of t picks (Marshall et al., 2005). This resulted in an average SWE uncertainty of approximately 10%.

2.3. GPR Data Analysis

We selected 13 transects to investigate forest boundary effects on SWE distribution in within-stand boundary areas. Transects were chosen that transitioned across forest boundaries to specifically examine within-stand boundary areas. The majority of these transects (12 of 13) were also chosen in the west-east orientation perpendicular to a north-south forest boundary as this was expected to have the largest influence from the prevailing westerly winds (Figure 3a). In total, this resulted in 10 windward within-stand boundary areas and 8 leeward within-stand boundary areas. These transects were analyzed to observe the variogram ranges of the entire transect (i.e., maximum distance of spatial autocorrelation between points) and coefficients of variation (COV) in a 50 m moving window. These parameters have been shown to indicate changes in spatial patterns of snow (Deems et al., 2006; Trujillo et al., 2007). The 50 m moving window size was chosen to have a relatively large sample size for each COV calculation, and 50 m is the approximate distance of the variogram range for all SnowEx transects with higher canopy cover percentages (McGrath et al., 2019). Further details toward the effect of the moving window size can be found in the supporting information (Text S1). It was observed that the 50 m moving window preserved the spatial patterns of COV while reducing the amplitude of variability in values (supporting information, Figures S1–S4).

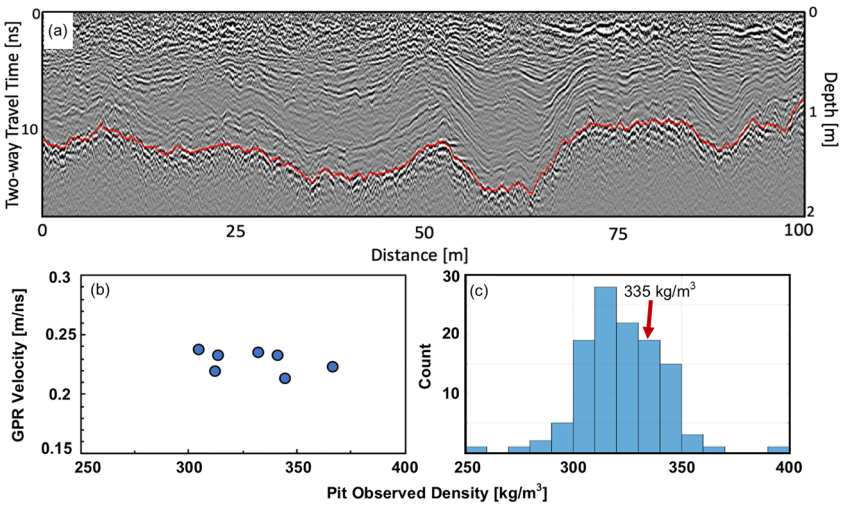

Figure 4. Ground-penetrating radar (GPR) data showing (a) an example radargram from Transect 3 with picked ground surface reflection shown in red, (b) mean density measurements from seven snow pits that were co-surveyed by the GPR unit used to determine median radar wave velocity and density, and (c) a histogram of all snow pit bulk density observations on Grand Mesa during the full 3 weeks of SnowEx17 (Elder et al., 2018) with the 335 kg/m^3 used for SWE calculations indicated.

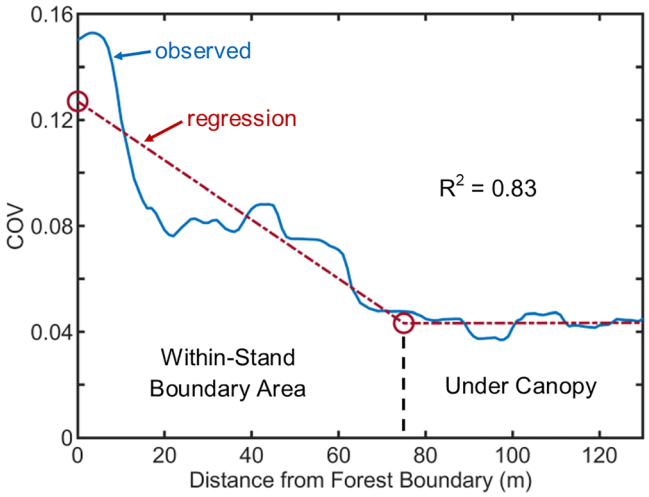

Figure 5. Example piecewise linear regression of SWE coefficient of variation (COV) data in a 50 m moving window relative to the distance from forest boundary used to determine the size of within-stand boundary areas as defined in Figure 1. Example data shown here are from Transect 3.

We quantified the length scale of boundary effects for within-stand boundary areas through observations of changes between under canopy conditions and conditions at the forest boundary. We primarily use COV changes due to the importance in considering this parameter when quantifying snow heterogeneity to improve simulated snow melt and streamflow (Clark et al., 2011; Luce et al., 1998, 1999). We plotted SWE COV as a distance from the forest boundary to as close to the center of the forest stand as available in transect data. The forest boundary is defined in this study as the location between forested and open areas with canopy height of 2 m in the Airborne Snow Observatory derived canopy data set (Painter, 2018). The length scale of within-stand boundary effects was determined using piecewise linear regression with a least squared approach. The breakpoint in the piecewise regression that produced the highest R-squared value while minimizing the linear slope after the breakpoint (representing background under canopy conditions) was used to determine the distance from the forest boundary that the boundary effects extend (Figure 5). Similar regressions have been utilized for many years to study within-stand boundary effects in ecological research (e.g., Alignier & Deconchat, 2013; Burton, 2002; Toms & Lesperance, 2003).

2.4. Statistical Analysis

We tested if the distribution patterns in the within-stand boundary areas and under canopy areas were statistically different using the Wilcoxon rank-sum test (Wilcoxon, 1945) that can be used interchangeably with the Mann–Whitney test (Helsel & Hirsch, 2002). We used this method to test the null hypothesis that data from the two data sets are from continuous distributions with equal medians at the 5% significance level. This test has been recently used to test for significant differences in snow depth (Currier & Lundquist, 2018); here we apply it to values of SWE and SWE COV.

3. Results

3.1. Within-Stand Boundary Effects

Analysis of the 13 transects displays the impact of a forest canopy on SWE distribution patterns. Four transects were chosen to illustrate representative conditions of a leeward forest boundary (Figure 6a), transects that include both windward and leeward forest boundaries for a longer stand (Figure 6b) and shorter stand (Figure 6c), and a windward forest boundary (Figure 6d). Variogram ranges were generally on the order of 10–50 m for transects under canopy increasing to around 100 m for transects that had a higher percentage of area in clearings, indicating higher variability of SWE distribution under canopy relative to clearings. Piecewise linear regression of SWE COV relative to distance from the forest boundary showed length scales of within-stand boundary areas (Figure 7 and supporting information, Figures S5 and S6). The largest length scale of within-stand boundary effects was in the leeward within-stand boundary area, ranging from 7 to 98 m (Table 2 and Figure 8) with a mean of 44 m (median of 48 m). In terms of mean canopy height along the transect (H), leeward within-stand boundary areas extended a mean of 4.3H (median of 4.0H; Table 2 and Figure 8). The length scale of boundary effects for windward within-stand boundary areas ranged from 2 to 55 m with a mean of 28 m (median of 26 m), or 3.7H (median of 3.6H). In forest stands that were lesser in length (as defined in Table 1), a stand length of 55 m produced boundary effects in both the windward and leeward within-stand boundary areas whereas a stand length of 30 m did not display clear boundary effects at our scale of analysis using a 50 m moving window for COV (Figure 6c). The shorter forest stand in Transect 33 also displays a continuing increase in SWE in the downwind direction, showing similarity to ribbon forests that are too short in the direction of wind for distribution patterns to settle. For this reason, and the size of our moving window, we only utilize forest stands with length greater than 50 m for further analysis. This results in a total of nine windward and seven leeward forest boundaries being used for the following analyses.

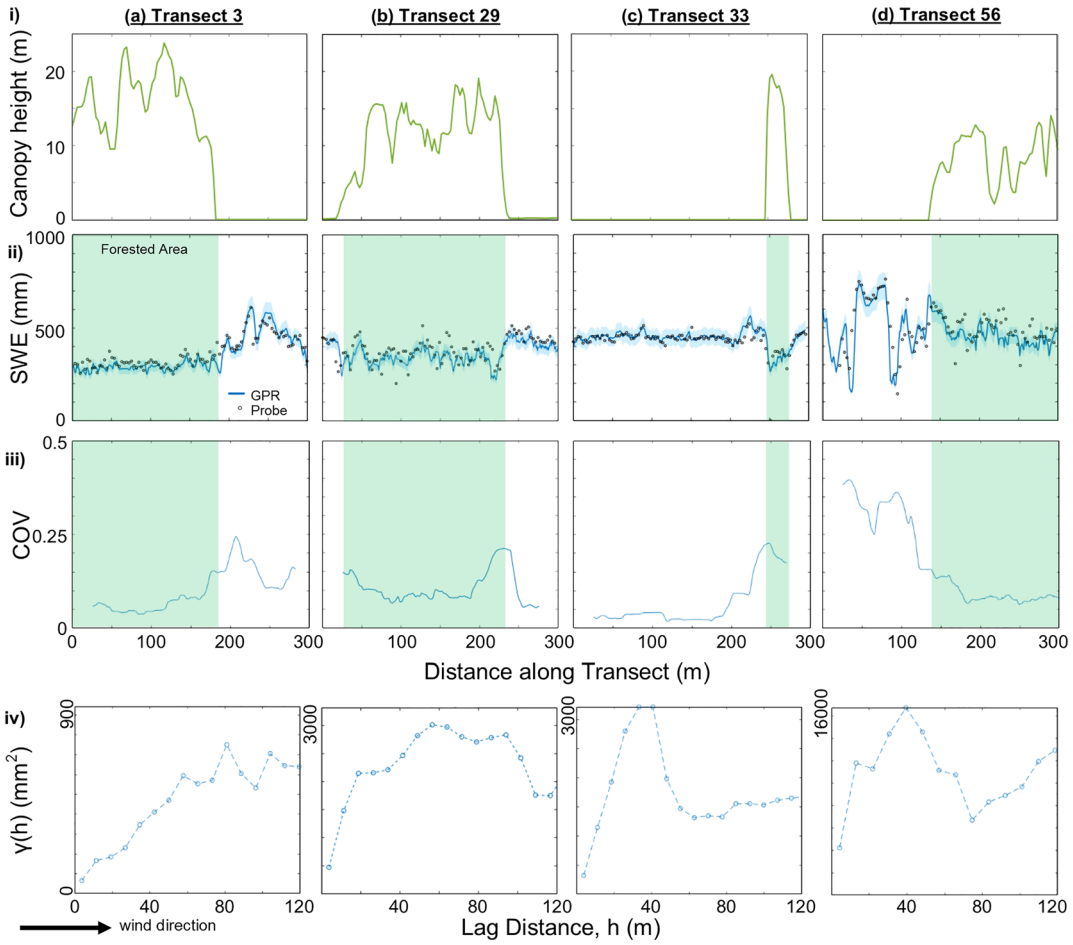

Figure 6. Data for Transects (a) 3, (b) 13, (c) 29, and (d) 56 showing (i) canopy height (Painter, 2018), (ii) SWE derived from ground-penetrating radar (GPR) and 3 m spaced snow depth probe observations (Brucker et al., 2018), (iii) SWE coefficient of variation (COV) in a 50 m moving window, and (iv) the variogram for the entire transect (note differences in *y*-axes). All data have been oriented such that wind direction is from left to right. Uncertainty bands in row (ii) were estimated using the range of observed bulk snow densities (Figure 4) and estimated accuracy of GPR picks. SWE estimates using snow depth probes for row (ii) were estimated by multiplying depth by the nearest pit observed snow density in similar canopy condition.

The SWE COV values were generally greater for the in-clearing and within-stand boundary areas relative to under canopy areas (Figures 6iii and 7) showing similar spatial patterns in variability as variograms (Figure 6iv). This is likely the result of snow drifting and/or scouring occurring in both the windward and leeward in-clearing boundary areas. Ground surface elevations indicate that the analyzed transects generally have gradually increasing elevations from west to east, with little to no topographic wind shielding affecting the within-stand boundary areas (supporting information, Figure S7). This suggests that the within-stand boundary effects observed are primarily a result of the forest stand. Stand parameters (canopy height, stand width, and stand length) did not correlate to within-stand boundary effects, though transects with windward forest boundaries used for this study tend to have lesser canopy heights than those with leeward forest boundaries. However, a larger number of within-stand boundary areas for analysis would be needed to provide statistical significance of these stand parameters.

The results from the Transect 49, oriented perpendicular to the dominant wind direction (i.e., north-south), showed within-stand boundary effects extending 6 m (~1H) displaying differing within-stand boundary effects, though the variogram range was similar to other transects. The north-south transect has a relatively large stand length of 565 m (Table 1). However, the stand widths are quite different with Transect 49 having a stand width of 850 m.

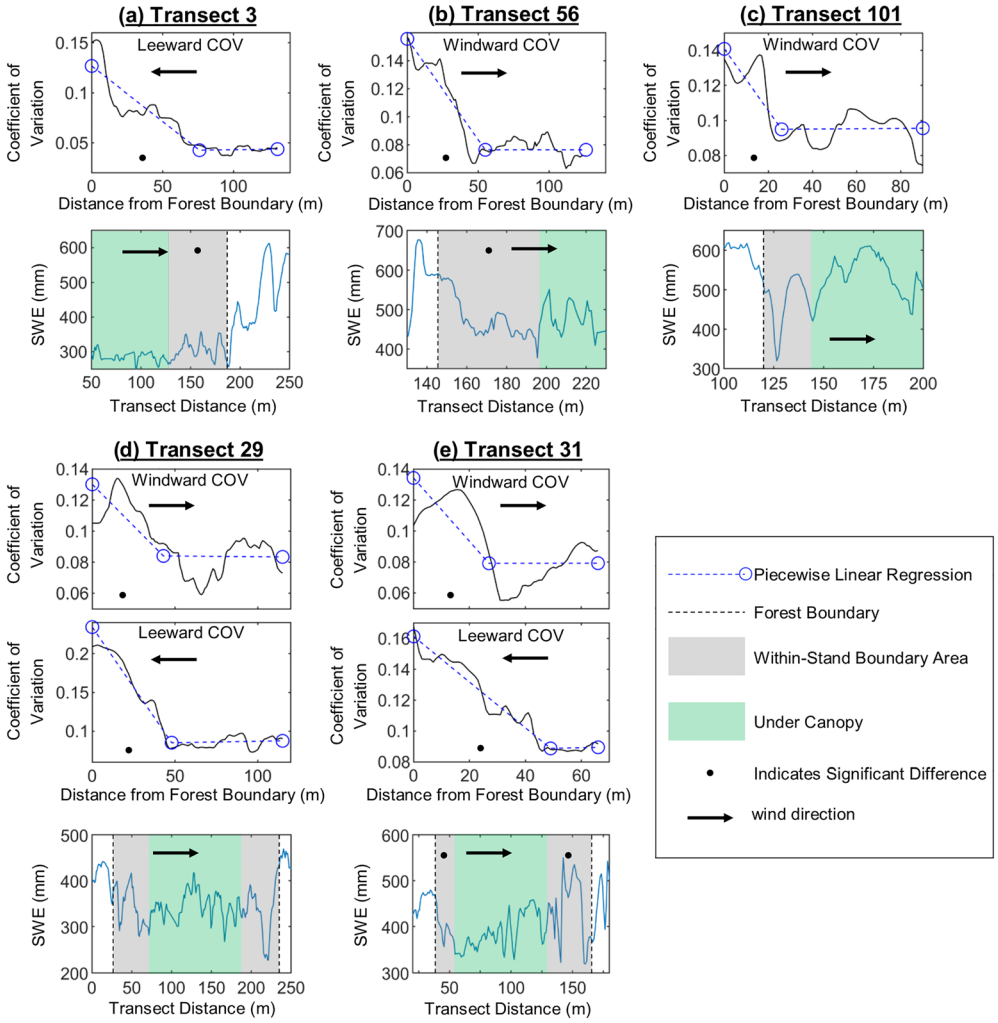

Figure 7. Results of the analyses showing the coefficient of variation (COV) with piecewise linear regressions and resulting boundary areas determined for Transects (a) 3, (b) 56, (c) 101, (d) 29, and (e) 31. Black dots in the within-stand boundary areas indicate significant differences between the marked within-stand boundary areas and the associated under canopy area at the 5% level using the Wilcoxon rank-sum test. Transect distance values are from the western-most point of each transect. Note the differences in the *y*-axes.

Statistical analysis shows that the SWE COV values are significantly different for all boundary areas determined in this study (Table 3). However, when comparing SWE values for within-stand boundary areas to under canopy values, five of the nine windward within-stand boundary areas and five out of seven leeward within-stand boundary areas were determined to be significantly different from under canopy values (Table 4). On average, SWE in windward and leeward within-stand boundary areas were 16 and 46 mm higher, respectively, compared to under canopy areas. Mean absolute differences were 32 and 74 mm, respectively. Similarly, mean differences in SWE COV were 0.014 and 0.020 (mean absolute differences of 0.025 and 0.035) for windward and leeward within-stand boundary areas relative to under canopy areas, respectively.

4. Discussion

The GPR data set collected during SnowEx17 on GM observed SWE distributions in forested areas and across forest boundaries, providing the unique opportunity to investigate spatial patterns in within-stand boundary areas. There has been limited previous work on this topic because forest cover can limit other remote sensing methods, with increasing errors under canopy (Harpold et al., 2014; Hopkinson et al., 2012; Tinkham

Table 2
Resulting Boundary Area Sizes as a Length and Ratio of Average Canopy Height Along the Transect (H)

Transect	Windward within-stand boundary area (m)	Windward within-stand boundary area (ratio of H)	Leeward within-stand boundary area (m)	Leeward within-stand boundary area (ratio of H)
3			**76**	**4.7**
13	**6**	**0.6**	**7**	**1.3**
15	25	2.3		
19	**2**	**0.2**	98	10.7
26			**15**	**1.3**
29	43	3.6	48	4.0
31	**27**	**3.2**	**49**	**5.7**
42	21	4.4	**12**	**2.5**
50	**51**	**5.6**		
56	**55**	**6.4**		
101	26	6.7		

Note. Values in bold text indicate significant differences between within-stand boundary areas and under canopy areas for both COV (Table 3) and SWE (Table 4) at the 5% level using the Wilcoxon rank-sum test. Only transects oriented east-west and those determined to have within-stand boundary areas at the scale of our analysis are shown here.

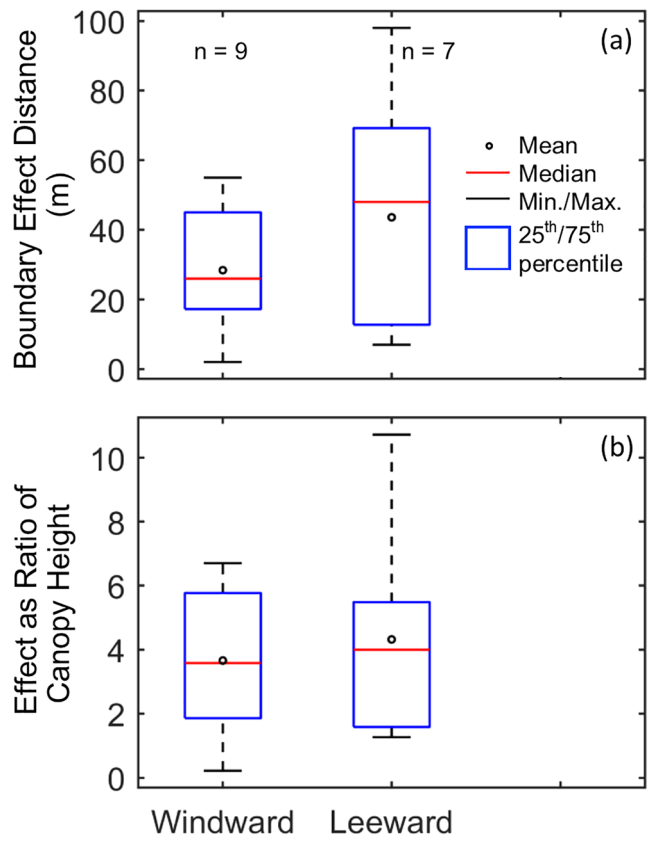

Figure 8. Boxplot summary of forest boundary effects for all windward and leeward within-stand boundary areas surveyed in the analyzed transects and presented as (a) distance from the forest boundary and (b) a ratio of mean stand canopy height.

et al., 2014). Often, analyses of snow distribution directly in forested areas are explicitly avoided using LiDAR products because of decimeter uncertainty in areas with denser canopy and instead focus on the influence of forests on adjacent locations in clearings (e.g., Currier & Lundquist, 2018). Recently airborne LiDAR mapping of snow depth under canopies has been greatly improved, though fine scale (1 m) depth products for GM during SnowEx17 still have gaps in data for forested areas that can range from 12% to 26% (Currier et al., 2019). Snow depth variability for in-clearing boundary areas has been recently shown to be significantly different for different environments (Currier & Lundquist, 2018), with the relative contributions of longwave radiation from the vegetation and shading from shortwave radiation showing differences over a range of snow climates. The GPR data presented here provide a spatially extensive data set that can and has been further used to assess airborne LiDAR observations during SnowEx17 (McGrath et al., 2019) and in turn enable further examination of spatial patterns such as within-stand boundary effects beyond individual transects on GM, depending on the canopy density and LiDAR retrieval properties.

The effect of vegetation on wind redistribution varies from the individual tree to stand (Revuelto et al., 2015), up to basin (Roth & Nolin, 2017) and regional (Tennant et al., 2017) spatial scales. At the scale of tens to hundreds of meters, as we investigate in this paper, previous work has focused on vegetation effects for in-clearing boundary areas that tend to form large snow drifts (Hiemstra et al., 2002, 2006). Our analysis shows the influence of boundary effects in within-stand boundary areas that are important for larger forest stands. We observed leeward within-stand boundary effects up to 98 m with a mean of 44 m (4.3H, Figure 8). This is over 50% greater than the observed windward within-stand boundary effect that resulted in a maximum of 55 m and a mean of 28 m (3.7H). It is important to note that the leeward within-stand boundary areas are only ~15% greater than windward within-stand boundary areas when considering the distance as a ratio to canopy height. Though these observations were conducted in tree islands on GM, a similar within-stand boundary effect at tree line for other locations is evident in previous studies. A similar length scale within-stand boundary effect can be observed in data presented by Trujillo et al. (2009), though not the focus of their study. Another example from Finland at a boundary between forest and tundra had a similar effect (Vajda et al., 2006). Golding and Swanson (1986) analyzed transect data across forest clearings and show clear within-stand boundary effects. These transect data display the transition of snow depth occurring over many tens of meters. However, the transects in Golding and Swanson (1986) continue only 1H to 2H into the forest stands and thus do not capture the full suite of areas found in this study (e.g., Figure 1). Therefore, direct estimation of within-stand boundary area of other studies for comparison are currently unavailable. However, these additional studies suggest that other forest stands have similar boundary areas of more than 2.0H, in agreement with our observations, thereby suggesting that our observations are not site specific. Though it is important to note the differences in boundary effects for different climate conditions observed by Currier and Lundquist (2018), as these physical processes are also influencing snow distribution in within-stand boundary areas. Thus, this topic merits further research to determine the length scale of these observed within-stand boundary effects for different canopy and

Table 3
The Coefficient of Variation Mean and Median Values for the Within-Stand Boundary and Under Canopy Areas

	Coefficient of variation					
	Mean			Median		
Transect	Windward within-stand boundary area	Under canopy	Leeward within-stand boundary area	Windward within-stand boundary area	Under canopy	Leeward within-stand boundary area
3		**0.043**	**0.085**		**0.044**	**0.08**
13	**0.316**	**0.282**	**0.26**	**0.317**	**0.289**	**0.26**
15	**0.123**	**0.142**		**0.122**	**0.143**	
19	**0.075**	**0.067**	**0.088**	**0.075**	**0.675**	**0.091**
26		**0.108**	**0.086**		**0.106**	**0.081**
29	**0.112**	**0.081**	**0.161**	**0.112**	**0.086**	**0.162**
31	**0.115**	**0.074**	**0.125**	**0.117**	**0.075**	**0.124**
42	**0.0663**	**0.071**	**0.064**	**0.068**	**0.072**	**0.064**
50	**0.085**	**0.113**		**0.087**	**0.095**	
56	**0.114**	**0.078**		**0.122**	**0.078**	
101	**0.119**	**0.094**		**0.124**	**0.097**	

Note. Values in bold text were found to be significantly different at the 5% level using the Wilcoxon rank-sum test for comparing within-stand boundary areas to under canopy areas. Note that all values in this table were found to be significant. Only transects oriented east-west and those determined to have within-stand boundary areas at the scale of our analysis are shown here.

climate/snowpack conditions. These different conditions may also require the use of algorithms more advanced than the simple piecewise linear regression that we successfully used in the present study. Collectively, the analyses presented here and in Currier and Lundquist (2018) highlight the influence of canopy effects at forest boundary areas and the need for further dedicated studies in the future.

The redistribution of snow from wind depends, in part, upon complex fluid dynamics in the forest canopy. These complex dynamics have been predominantly investigated on the windward forest boundary (Belcher et al., 2008; Dupont & Brunet, 2008; Tischmacher & Ruck, 2013). Belcher et al. (2003) discuss the theoretical adjustment of effective roughness length parameters with fetch relative to the boundary layer, showing results that indicate different wind patterns at the windward and leeward boundary areas of a forest stand based on field data and wind tunnel experiments. When comparing boundary effects between Belcher et al. (2003) and the SWE distribution patterns observed on GM, similarities in the relative scale of effective roughness changes and within-stand boundary effects on SWE distribution patterns occur. Furthermore, Detto et al. (2008) show the turbulence dynamics at the leeward side of a forest stand that could further explain the larger leeward within-stand boundary effects observed.

Table 4
The Snow Water Equivalent Mean and Median Values for the Within-Stand Boundary and Under Canopy Areas

	Snow water equivalent (mm)					
	Mean			Median		
Transect	Windward within-stand boundary area	Under canopy	Leeward within-stand boundary area	Windward within-stand boundary area	Under canopy	Leeward within-stand boundary area
3		**285**	**299**		**288**	**295**
13	**282**	**325**	**628**	**285**	**276**	**551**
15	290	284		284	272	
19	**404**	**360**	352	**403**	**365**	357
26		**346**	**446**		**343**	**443**
29	342	342	333	338	340	336
31	**390**	**413**	**378**	**382**	**403**	**372**
42	522	**516**	**470**	510	**512**	**463**
50	**553**	**447**		**563**	**455**	
56	**498**	**443**		**475**	**443**	
101	579	582		578	585	

Note. Values in bold text were found to be significant at the 5% level using the Wilcoxon rank-sum test. Only transects oriented east-west and those determined to have within-stand boundary areas at the scale of our analysis are shown here.

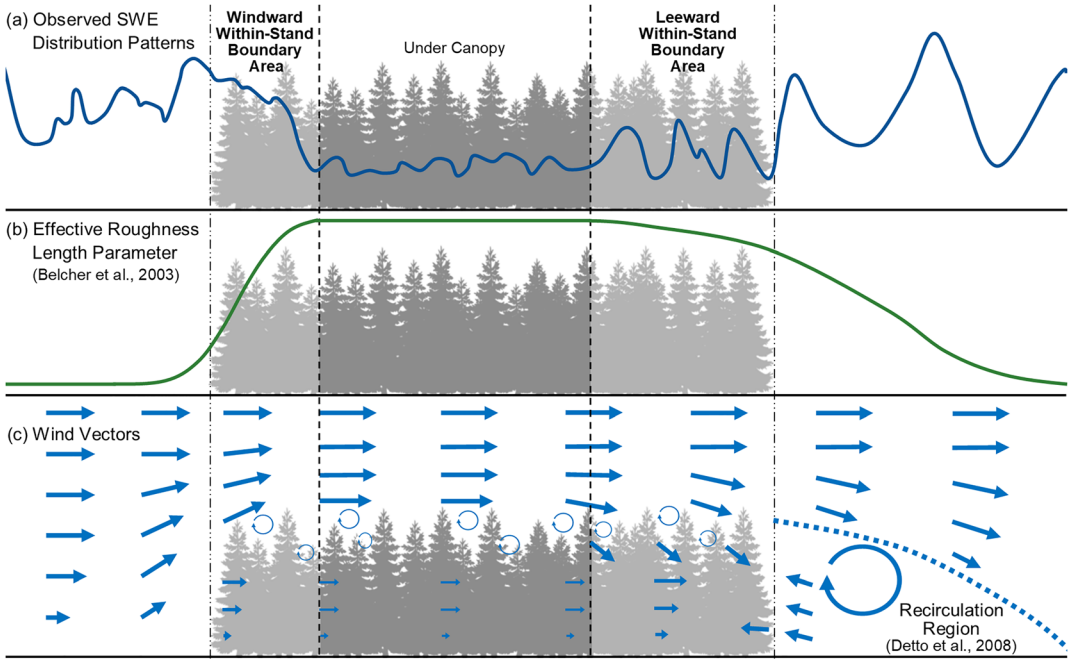

Figure 9. Conceptual diagram of the wind dynamics that occur around a forest stand in the direction of wind. Shown here is (a) representative pattern of snow water equivalent (SWE) distribution observed in this study using relative depths of Transect 56 for the windward edge and boundary effect and Transect 3 for the middle section, leeward boundary effect, and leeward edge, (b) the relative effective roughness length parameter when adjusted for fetch along the distance of a forest stand (Belcher et al., 2003), and (c) wind vectors that are expected as a result of the effective roughness length parameter and recirculation region on the leeward edge of the stand (Detto et al., 2008).

These studies on the complex wind dynamics that occur around and within a forest stand form a conceptualization of how the within-stand boundary effects on snow distribution may form (Figure 9). The windward forest boundary will create an abrupt upward angle in wind vectors from a rapid increase in effective roughness length. This feature causes a sharp decline in wind speed over a short distance in the windward within-stand boundary area (Belcher et al., 2003; Dupont & Brunet, 2008; Tischmacher & Ruck, 2013). The effective roughness length reaches a steady maximum value above the under canopy area of the stand. The effective roughness length parameter then begins a gradual decline in the leeward within-stand boundary area, allowing wind vectors to begin angling toward the ground. Additionally, a large eddy forms in the leeward in-clearing boundary area for a horizontal distance of 2–5H (Detto et al., 2008). This eddy, or recirculation region, will have a wind structure that can have wind vectors re-entering the forest stand along with the downward angled wind vectors from the top of the canopy (Figure 9c). These processes at the leeward within-stand and leeward in-clearing boundary areas, based on Belcher et al. (2003) and Detto et al. (2008), create a leeward within-stand boundary area environment that has a larger length scale relative to that which occurs at the windward within-stand boundary area, explaining the magnitude of within-stand boundary effects observed in our study (Figures 8 and 9). These wind dynamics will impact the distribution of SWE during snowfall events, redistribution of snow in tree canopies, and redistribution from in-clearing to within-stand boundary and under canopy areas. It is unlikely that snow under a forest canopy is redistributed due to the increased effective roughness length parameter that decreases under-canopy wind speeds. However, there is much work that could be done to further understand the complex fluid dynamics that occur in the wind field during winter periods and how this relates to the wind redistribution and of snow and energy fluxes in a forested area. For example, further investigations are warranted at within-stand boundary areas oriented parallel to wind direction, with less consistent wind directions, and different canopy architectures that likely alter the scale of these influences (e.g., Cassiani et al., 2008; Kanani-Sühring & Raasch, 2015).

Alternative hypotheses considered to explain the observed variability include forest canopy structure effects on wind fields. We analyzed the available canopy height data using piecewise linear regression that showed

no correlation to observed within-stand boundary effects (supporting information, Figure S12a). Additionally, we compared the horizontal distance of younger trees around the edges into the stand from the forest boundary and similarly found no correlation (supporting information, Figure S12b). Furthermore, canopy density changes in a similar pattern as canopy height along the observed transects suggesting that this is not likely a major factor either. Energy fluxes such as shortwave radiation penetration into the forest stand can be important for SWE distribution processes during accumulation, though less likely to impact east-west distributions (focus of our study) compared to north-south distributions. Energy fluxes may play a stronger role in within-stand boundary areas for north-south transects during the spring melt season at magnitudes described below (e.g., Musselman et al., 2008). Future work could incorporate further analyses of LiDAR point cloud data, canopy density, energy balance modeling, and high-density instrumentation to further investigate the within-stand boundary areas in the field. Additionally, wind tunnel studies may provide valuable insights toward factors such as canopy density, canopy structure, and wind speeds on within-stand boundary area SWE distribution.

Our results of within-stand boundary areas compare well with known wind deposition for in-clearing areas. Previous work has shown that wind-related deposition downwind of a forest can extend 3H to 10H (Brandle & Finch, 1991; Hiemstra et al., 2002, 2006; Tabler, 2003). The mean within-stand boundary areas that we observed are at the lower end of this range with 3.7H and 4.3H for windward and leeward within-stand boundary areas, respectively. Other energy budget components tend to have influences at lesser length scales than our observed within-stand boundary areas (Currier & Lundquist, 2018). Enhanced longwave radiation from the canopy has an influence of 0.5H (Lawler & Link, 2011; Musselman & Pomeroy, 2017; Seyednasrollah & Kumar, 2014; Webster et al., 2016; Woo & Giesbrecht, 2000) whereas forest shading of shortwave radiation extends 0.5H to 2.0H (Lawler & Link, 2011; Musselman et al., 2015; Seyednasrollah & Kumar, 2014).

Current representation of snow redistribution in process-based models is dominantly driven by topography. Explicit redistribution of snow across complex topography can be represented with multiple approaches including simple terrain-based parameters (e.g., Winstral et al., 2002), semi-empirical parameterizations of vertically integrated snow transport rates, and schemes that fully resolve the 3-D turbulent-diffusion of blowing snow (i.e., Mott et al., 2018). However, snow redistribution within forest stands have yet to be as thoroughly examined as terrain-based approaches. Most models include wind speed reduction in forested pixels (e.g., SnowPalm, Broxton et al., 2015) but do not model the patterns of wind flow through forests and around individual trees due to computational limitations. To represent snow drifts that form in open areas on the leeside of forests, some modeling efforts have treated trees as roughness elements (i.e., as part of the terrain) by including canopy height in the digital elevation model (Deems, 2007; Hiemstra et al., 2002, 2006). These efforts have focused on ribbon forests with relatively narrow profiles that could be treated as a wind break similar to a snow fence. However, wind flow dynamics within larger forest stands, at the forest boundaries, and the impacts on snow redistribution have yet to be attempted in modeling analyses. Prior high-resolution modeling analyses of snow in forests have focused on classified zones with respect to canopy (e.g., Broxton et al., 2015) but with no consideration of windward or leeward within-stand boundary areas. In an auxiliary analysis (see Text S2), we assessed whether the well-developed SnowModel (Liston et al., 2007; Liston & Elder, 2006; Liston & Sturm, 1998), using available data (Skiles, 2018), captured the boundary effects within a forest stand, and whether a high spatial resolution in the model is necessary to do so. All snow models (to our knowledge) lack the complex wind dynamics on the leeward side of forests (Figure 9), but it is possible for current models to capture the windward within-stand boundary effect due to the reduction of wind speed that occurs when transitioning from open areas to a forested area. Indeed, the supplemental modeling experiment confirms that the within-stand boundary effects on SWE are reproduced in windward areas but not in leeward areas, which illustrates the need for more process understanding and model development.

Furthermore, when validating model data for forested areas, it is important to use under canopy conditions and not within-stand boundary areas. The model error may be overestimated or incorrectly assess simulation bias (i.e., result in a negative bias when a positive bias is more accurate) based on field measurements in within-stand boundary areas and not under canopy conditions (supporting information, Figures S7 and S8). To include these within-stand boundary areas, more complex simulations of wind flow in forests (e.g., recirculation at the leeward forest boundary) could be achieved with atmospheric model output or coupled 3-D fluid dynamics models, but with added computational expense.

When considering the forest stand boundary effects on SWE distribution from a watershed-scale modeling perspective, lumped parameters that include within-stand boundary areas of forest stands could prove beneficial. Based on the observations presented in these data, along with other data that suggest similar boundary effects likely occur elsewhere (Trujillo et al., 2009; Vajda et al., 2006), a 4.0H to 4.5H leeward within-stand boundary area and 3.5H to 4.0H windward within-stand boundary area could be used. In addition to the observed within-stand boundary effects in mid-winter SWE distributions, these areas will have different energy balance components that further support an additional area of parameters for modeling purposes (e.g., Andreadis et al., 2009; Musselman, Molotch, Margulis, Kirchner, et al., 2012). In particular, including sub-element variability as parameterized by COV can improve snowmelt and runoff in simulations (Clark et al., 2011; Luce et al., 1998, 1999). Incorporating these additional within-stand boundary areas into a lumped parameter model could prove beneficial, though further studies are necessary to quantify this benefit.

Furthermore, to quantify conditions under canopy in a forested area, instrumentation and measurements should occur at least 50 m and potentially up to 100 m from the forest boundary, depending on wind direction. In terms of a factor to mean stand canopy height, these values are approximately 6.7H and 10.7H, respectively. This distance would ensure that boundary effects are not impacting measurements and more representative under canopy conditions are being observed. Though the observations presented herein were collected during a short period relative to the time of snow cover (Figure 3b), the within-stand boundary effects are likely to occur over the entire snow covered season due to (1) the consistent wind direction on GM (Figure 3a), (2) the similar patterns of snow depth differences observed between multiple sensors under varying canopy conditions the entire time of snow cover (Figure 3b), and (3) wind profile dynamics that are being interpreted as the cause of the observed within-stand boundary effects will be based on stand parameters that are constant at this spatiotemporal scale (Figure 8). However, factors such as exposure, topography, subsequent burial of sub-canopy, canopy architecture at the individual tree and stand scales, and advanced regeneration need to also be considered. Additionally, further investigations toward the scale of similar within-stand boundary areas during the melt season with potentially stronger influences from energy balance factors are merited.

Future investigations and modeling studies could benefit from considering the within-stand boundary effects on forested area snow distributions shown in this paper. Additionally, survey design and instrumentation site selection could be improved for forested areas through consideration of the length scales of boundary effects that we observed. The data presented herein could also be useful to assess airborne instruments to further investigate the boundary effects across GM during SnowEx17. It is important to further investigate the controlling parameters on the observed within-stand boundary effects for future applications. We recommend these investigations utilize empirical observations, modeling, and wind tunnel experiments to target parameters such as, but not limited to, canopy architecture, canopy health, tree species, wind speed and direction (at multiple heights), topographic influences, climate type, and ground cover vegetation type and height.

5. Conclusions

The GPR data set collected during SnowEx17 on GM provides data that reveal spatial SWE patterns in within-stand boundary areas. These data provide high-resolution observations (i.e., multiple observations per meter) at larger spatial extents (i.e., hundreds of meters) than any other ground-based measurements for assessing airborne sensors flown during SnowEx17. The within-stand boundary area spatial patterns observed display boundary effects that occur at varying scales depending on the wind direction relative to the stand. Utilizing a moving window for COV values, we determined the windward within-stand boundary area to have a length scale which ranged from 2 to 55 m with a mean of 28 m. In terms of mean canopy heights, these distances represent a range of 0.2H to 6.7H and a mean of 3.7H. The leeward within-stand boundary area length scale ranged from 7 to 98 m with a mean of 44 m. In terms of mean canopy heights, these distances represent a range of 0.7H to 10.7H and a mean of 4.3H. We present a conceptual framework of the complex wind dynamics that occur in the direction of wind with a forest stand to explain the observed within-stand boundary effects. Future investigations could improve understanding of this complex process and parameterize the driving variables of these patterns. Additionally, future survey designs and instrument deployments will benefit from considering within-stand boundary effects to ensure observations of the intended conditions.

Data Availability Statement

Data from the NASA SnowEx campaign can be found online through the National Snow and Ice Data Center (https://nsidc.org/data/snowex). Citations for specific data sets can be found in the references section.

Acknowledgments

We would like to acknowledge the anonymous reviewers that provided constructive feedback on earlier versions of this manuscript. Their input has greatly improved the presentation of this study. Additionally, the feedback provided by the anonymous Associate Editor as well as Editor Jessica Lundquist was helpful in revising our manuscript. Funding for the collection, processing, and analysis of the presented data set were provided by National Aeronautics and Space Administration (NASA) THP Award 80NSSC18K0877 and National Science Foundation (NSF) EAR Award 1624853. Funding for the snow model analyses was provided by NSF EAR Award 1761441 and NASA THP Award NNX17AL41G. The authors would also like to recognize the tremendous effort that the SnowEx leadership team provided to coordinate the field and airborne campaign during SnowEx17. We would also like to extend our appreciation to the numerous scientists that volunteered for the field efforts during the campaign. Without these combined efforts, the SnowEx data set would not be nearly as complete. Additionally, we would like to recognize the ongoing efforts in to improve SnowModel.

References

Alignier, A., & Deconchat, M. (2013). Patterns of forest vegetation to edge effect as revealed by a continuous approach. *Annals of Forest Science*, *70*(6), 601–609. https://doi.org/10.1007/s13595-013-0301-0

Andreadis, K. M., Storck, P., & Lettenmaier, D. P. (2009). Modeling snow accumulation and ablation processes in forested environments. *Water Resources Research*, *45*, W05429. https://doi.org/10.1029/2008WR007042

Bair, E., Rittger, K., Davis, R., Painter, T., & Dozier, J. (2016). Validating reconstruction of snow water equivalent in California's Sierra Nevada using measurements from the NASA Airborne Snow Observatory. *Water Resources Research*, *52*, 8437–8460. https://doi.org/10.1002/2016WR018704

Barnhart, T., Molotch, N., Livneh, B., Harpold, A., Knowles, J., & Schneider, D. (2016). Snowmelt rate dictates streamflow. *Geophysical Research Letters*, *43*, 8006–8016. https://doi.org/10.1002/2016GL069690

Belcher, S., Finnigan, J., & Harman, I. (2008). Flows through forest canopies in complex terrain. *Ecological Applications*, *18*(6), 1436–1453. https://doi.org/10.1890/06-1894.1

Belcher, S., Jerram, N., & Hunt, J. (2003). Adjustment of a turbulent boundary layer to a canopy of roughness elements. *Journal of Fluid Mechanics*, *488*, 369, S0022112003005019–398. https://doi.org/10.1017/S0022112003005019

Blöschl, G. (1999). Scaling issues in snow hydrology. *Hydrological Processes*, *13*(14–15), 2149–2175. https://doi.org/10.1002/(SICI)1099-1085(199910)13:14/15<2149::AID-HYP847>3.0.CO;2-8

Bradford, J., Harper, J., & Brown, J. (2009). Complex dielectric permittivity measurements from ground-penetrating radar data to estimate snow liquid water content in the pendular regime. *Water Resources Research*, *45*, W08403. https://doi.org/10.1029/2008WR007341

Brandle, J.R., Finch, S. (1991). How windbreaks work. Natural Resources, Nebraska Cooperative Extension Service. National Agroforesty Center. 91-1763-B

Broxton, P. D., Harpold, A. A., Biederman, J. A., Troch, P. A., Molotch, N. P., & Brooks, P. D. (2015). Quantifying the effects of vegetation structure on snow accumulation and ablation in mixed-conifer forests. *Ecohydrology*, *8*(6), 1073–1094. https://doi.org/10.1002/eco.1565

Brucker, L., Hiemstra, C., Marshall, H. P., & Elder, K. (2018). SnowEx community snow depth probe measurements, version 1, edited by NASA NSIDC, Boulder, Colorado USA. https://doi.org/10.5067/WKC6VFMT7JTF

Brucker, L., Hiemstra, C., Marshall, H. P., Elder, K., De Roo, R., Mousavi, M., et al. (2017). A first overview of SnowEx ground-based remote sensing activities during the winter 2016–2017, in *2017 IEEE International Geoscience and Remote Sensing Symposium (IGARSS)* (pp. 1391–1394).

Bühler, Y., Adams, M., Bosch, R., & Stoffel, A. (2016). Mapping snow depth in alpine terrain with unmanned aerial systems (UASs): Potential and limitations. *The Cryosphere*, *10*(3), 1075–1088. https://doi.org/10.5194/tc-10-1075-2016

Bühler, Y., Marty, M., Egli, L., Veitinger, J., Jonas, T., Thee, P., & Ginzler, C. (2015). Snow depth mapping in high-alpine catchments using digital photogrammetry. *The Cryosphere*, *9*(1), 229–243. https://doi.org/10.5194/tc-9-229-2015

Burton, P. (2002). Effects of clearcut edges on trees in the sub-boreal spruce one of northwest-central British Columbia. *Silva Fennica*, *36*(1), 329–352.

Cassiani, M., Katul, G. G., & Albertson, J. D. (2008). The effects of canopy leaf area index on airflow across forest edges: Large-eddy simulation and analytical results. *Boundary-Layer Meteorology*, *126*(3), 433–460. https://doi.org/10.1007/s10546-007-9242-1

Clair, J., & Holbrook, W. (2017). Measuring snow water equivalent from common-offset GPR records through migration velocity analysis. *The Cryosphere*, *11*(6), 2997–3009. https://doi.org/10.5194/tc-11-2997-2017

Clark, M., Hendrikx, J., Slater, A., Kavetski, D., Anderson, B., Cullen, N., et al. (2011). Representing spatial variability of snow water equivalent in hydrologic and land-surface models: A review. *Water Resources Research*, *47*, W07539. https://doi.org/10.1029/2011WR010745

Currier, W. R., & Lundquist, J. D. (2018). Snow depth variability at the forest edge in multiple climates in the western United States. *Water Resources Research*, *54*, 8756–8773. https://doi.org/10.1029/2018WR022553

Currier, W. R., Pflug, J., Mazzotti, G., Jonas, T., Deems, J. S., Bormann, K. J., et al. (2019). Comparing aerial lidar observations with terrestrial lidar and snow-probe transects from NASA's 2017 SnowEx campaign. *Water Resources Research*, *55*(7), 6285–6294. https://doi.org/10.1029/2018WR024533

Deems, J. (2007). Quantifying scale relationships in snow distributions, Colorado State University Dissertation, Department of Geosciences.

Deems, J., Fassnacht, S., & Elder, K. (2006). Fractal distribution of snow depth from lidar data. *Journal of Hydrometeorology*, *7*(2), 285–297. https://doi.org/10.1175/JHM487.1

Detto, M., Katul, G., Siqueira, M., Juang, J., & Stoy, P. (2008). The structure of turbulence near a tall forest edge: The backward-facing step flow analogy revisited. *Ecological Applications*, *18*(6), 1420–1435. https://doi.org/10.1890/06-0920.1

Dozier, J., Bair, E., & Davis, R. (2016). Estimating the spatial distribution of snow water equivalent in the world's mountains. *Wiley Interdisciplinary Reviews Water*, *3*(3), 461–474. https://doi.org/10.1002/wat2.1140

Dupont, S., & Brunet, Y. (2008). Impact of forest edge shape on tree stability: A large-eddy simulation study. *Forestry*, *81*(3), 299–315. https://doi.org/10.1093/forestry/cpn006

Elder, K., Brucker, L., Hiemstra, C., & Marshall, H. P. (2018). SnowEx17 community snow pit measurements, version 1, edited by NASA NSIDC, Boulder, Colorado USA. https://doi.org/10.5067/Q0310G10G1XULZS

Elder, K., Dozier, J., & Michaelsen, J. (1991). Snow accumulation and distribution in an alpine watershed. *Water Resources Research*, *27*(7), 1541–1552. https://doi.org/10.1029/91WR00506

Elder, K., Rosenthal, W., & Davis, R. (1998). Estimating the spatial distribution of snow water equivalence in a montane watershed. *Hydrological Processes*, *12*(10–11), 1793–1808. https://doi.org/10.1002/(SICI)1099-1085(199808/09)12:10/11<1793::AID-HYP695>3.0.CO;2-K

Ellerbruch, D. A., & Boyne, H. S. (1980). Snow stratigraphy and water equivalence measured with an active microwave system. *Journal of Glaciology*, *26*(94), 225–233. https://doi.org/10.1017/S0022143000010765

Frei, A., Tedesco, M., Lee, S., Foster, J., Hall, D., Kelly, R., & Robinson, D. (2012). A review of global satellite-derived snow products. *Advances in Space Research*, *50*(8), 1007–1029. https://doi.org/10.1016/j.asr.2011.12.021

Golding, D. L., & Swanson, R. H. (1986). Snow distribution patterns in clearings and adjacent forest. *Water Resources Research*, *22*(13), 1931–1940. https://doi.org/10.1029/wr022i013p01931

Gosz, J. R. (1993). Ecotone hierarchies. *Ecological Applications*, *3*(3), 369–376. https://doi.org/10.2307/1941905

Gouttevin, I., Lehning, M., Jonas, T., Gustafsson, D., & Molder, M. (2015). A two-layer canopy model with thermal inertia for an improved snowpack energy balance below needleleaf forest (model SNOWPACK, version 3.2.1, revision 741). *Geoscientific Model Development*, *8*(8), 2379–2398. https://doi.org/10.5194/gmd-8-2379-2015

Griessinger, N., Mohr, F., & Jonas, T. (2018). Measuring snow ablation rates in alpine terrain with a mobile multioffset ground-penetrating radar system. *Hydrological Processes*, *32*(21), 3272–3282. https://doi.org/10.1002/hyp.13259

Gubler, H., & Hiller, M. (1984). The use of microwave FMCW radar in snow and avalanche research. *Cold Regions Science and Technology*, *9*(2), 109–119. https://doi.org/10.1016/0165-232X(84)90003-X

Harpold, A. A., Biederman, J. A., Condon, K., Merino, M., Korgaonkar, Y., Nan, T., et al. (2014). Changes in snow accumulation and ablation following the Las Conchas Forest Fire, New Mexico, USA. *Ecohydrology*, *7*(2), 440–452. https://doi.org/10.1002/eco.1363

Heilig, A., Schneebeli, M., & Eisen, O. (2009). Upward-looking ground-penetrating radar for monitoring snowpack stratigraphy. *Cold Regions Science and Technology*, *59*(2–3), 152–162. https://doi.org/10.1016/j.coldregions.2009.07.008

Helsel, D. R., & Hirsch, R. M. (2002). Statistical methods in water resources (Vol. 4, pp. 1–524). U.S: Geological Survey. Retrieved from https://pubs.usgs.gov/twri/twri4a3/

Hiemstra, C., Liston, G., & Reiners, W. (2002). Snow redistribution by wind and interactions with vegetation at upper treeline in the Medicine Bow Mountains, Wyoming, USA. *Arctic Antarctic and Alpine Research*, *34*(3), 262–273. https://doi.org/10.2307/1552483

Hiemstra, C., Liston, G., & Reiners, W. (2006). Observing, modelling, and validating snow redistribution by wind in a Wyoming upper treeline landscape. *Ecological Modelling*, *197*(1–2), 35–51. https://doi.org/10.1016/j.ecolmodel.2006.03.005

Hopkinson, C., Collins, T., Anderson, A., Pomeroy, J., & Spooner, I. (2012). Spatial snow depth assessment using LiDAR transect samples and public GIS data layers in the Elbow River watershed, Alberta. *Canadian Water Resources Journal*, *37*(2), 69–87. https://doi.org/10.4296/cwrj3702893

Jencso, K. G., & McGlynn, B. L. (2011). Hierarchical controls on runoff generation: Topographically driven hydrologic connectivity, geology, and vegetation. *Water Resources Research*, *47*, W11527. https://doi.org/10.1029/2011wr010666

Jennings, K. S., Barnhart, T. B., & Molotch, N. P. (2018). SnowEx17 time series sonic snow depth measurement array, version 1, edited by NASA NSIDC, Boulder, Colorado USA. https://doi.org/10.5067/5YJEYNLS1YK4

Kanani-Sühring, F., & Raasch, S. (2015). Spatial variability of scalar concentrations and fluxes downstream of a clearing-to-forest transition: A large-eddy simulation study. *Boundary-Layer Meteorology*, *155*(1), 1–27. https://doi.org/10.1007/s10546-014-9986-3

Kim, E. (2018). How can we find out how much snow is in the world? *Eos*, *99*(June), 2–7. https://doi.org/10.1029/2018EO099939

Kim, E., Gatebe, C., Hall, D., Newlin, J., Misakonis, A., Elder, K., et al. (2017). NASA's SnowEx campaign: Observing seasonal snow in a forested environment. In 2017 IEEE International Geoscience and Remote Sensing Symposium (IGARSS) (pp. 1388–1390). IEEE. https://doi.org/10.1109/IGARSS.2017.8127222

Lawler, R. R., & Link, T. E. (2011). Quantification of incoming all-wave radiation in discontinuous forest canopies with application to snowmelt prediction. *Hydrological Processes*, *25*(21), 3322–3331. https://doi.org/10.1002/hyp.8150

Liston, G. E., & Elder, K. (2006). A distributed snow-evolution modeling system (SnowModel). *Journal of Hydrometeorology*, *7*(6), 1259–1276. https://doi.org/10.1175/JHM548.1

Liston, G. E., Haehnel, R. B., Sturm, M., Hiemstra, C. A., Berezovskaya, S., & Tabler, R. D. (2007). Simulating complex snow distributions in windy environments using SnowTran-3D. *Journal of Glaciology*, *53*(181), 241–256. https://doi.org/10.3189/172756507782202865

Liston, G. E., & Sturm, M. (1998). A snow-transport model for complex terrain. *Journal of Glaciology*, *44*(148), 498–516. https://doi.org/10.1017/S0022143000002021

Lopez-Moreno, J. I., & Latron, J. (2008). Influence of canopy density on snow distribution in a temperate mountain range. *Hydrological Processes*, *22*(1), 117–126. https://doi.org/10.1002/hyp.6572

Luce, C. H., Tarboton, D. G., & Cooley, K. R. (1998). The influence of the spatial distribution of snow on basin-averaged snowmelt. *Hydrological Processes*, *12*(10–11), 1671–1683. https://doi.org/10.1002/(SICI)1099-1085(199808/09)12:10/11<1671::AID-HYP688>3.0.CO;2-N

Luce, C. H., Tarboton, D. G., & Cooley, K. R. (1999). Sub-grid parameterization of snow distribution for an energy and mass balance snow cover model. *Hydrological Processes*, *13*(12–13), 1921–1933. https://doi.org/10.1002/(SICI)1099-1085(199909)13:12/13<1921::AID-HYP867>3.0.CO;2-S

Lundberg, A., Ala-Aho, P., Eklo, O., Klove, B., Kvaerner, J., & Stumpp, C. (2016). Snow and frost: Implications for spatiotemporal infiltration patterns—A review. *Hydrological Processes*, *30*(8), 1230–1250. https://doi.org/10.1002/hyp.10703

Lundquist, J., & Dettinger, M. (2005). How snowpack heterogeneity affects diurnal streamflow timing. *Water Resources Research*, *41*, W05007. https://doi.org/10.1029/2004WR003649

Lundquist, J., Dickerson-Lange, S., Lutz, J., & Cristea, N. (2013). Lower forest density enhances snow retention in regions with warmer winters: A global framework developed from plot-scale observations and modeling. *Water Resources Research*, *49*, 6356–6370. https://doi.org/10.1002/wrcr.20504

Mankin, J., Viviroli, D., Singh, D., Hoekstra, A., & Diffenbaugh, N. (2015). The potential for snow to supply human water demand in the present and future. *Environmental Research Letters*, *10*(11), 114016. https://doi.org/10.1088/1748-9326/10/11/114016

Marshall, H., & Koh, G. (2008). FMCW radars for snow research. *Cold Regions Science and Technology*, *52*(2), 118–131. https://doi.org/10.1016/j.coldregions.2007.04.008

Marshall, H., Koh, G., Forster, R., & MacAyeal, D. (2005). Estimating alpine snowpack properties using FMCW radar. *Annals of Glaciology*, *40*, 157–162. https://doi.org/10.3189/172756405781813500

Marshall, H., Schneebeli, M., & Koh, G. (2007). Snow stratigraphy measurements with high-frequency FMCW radar: Comparison with snow micro-penetrometer. *Cold Regions Science and Technology*, *47*(1–2), 108–117. https://doi.org/10.1016/j.coldregions.2006.08.008

McGrath, D., Sass, L., O'Neel, S., Arendt, A., Wolken, G., Gusmeroli, A., et al. (2015). End-of-winter snow depth variability on glaciers in Alaska. *Journal of Geophysical Research: Earth Surface*, *120*, 1530–1550. https://doi.org/10.1002/2015JF003539

McGrath, D., Webb, R. W., Shean, D., Bonnell, R., Marshall, H. P., Painter, T., et al. (2019). Spatially extensive ground-penetrating radar snow depth observations during NASA's 2017 SnowEx campaign: Comparison with in situ, airborne, and satellite observations. *Water Resources Research*, *55*, 10,026–10,036. https://doi.org/10.1029/2019WR024907

McNamara, J. P., Chandler, D., Seyfried, M., & Achet, S. (2005). Soil moisture states, lateral flow, and streamflow generation in a semi-arid, snowmelt-driven catchment. *Hydrological Processes*, *19*(20), 4023–4038. https://doi.org/10.1002/hyp.5869

Moeser, D., Mazzotti, G., Helbig, N., & Jonas, T. (2016). Representing spatial variability of forest snow: Implementation of a new interception model. *Water Resources Research*, *52*, 1208–1226. https://doi.org/10.1002/2015wr017961

Molotch, N. P., & Meromy, L. (2014). Physiographic and climatic controls on snow cover persistence in the Sierra Nevada Mountains. *Hydrological Processes*, *28*(16), 4573–4586. https://doi.org/10.1002/hyp.10254

Mott, R., Vionnet, V., & Grünewald, T. (2018). The seasonal snow cover dynamics: Review on wind-driven coupling processes. *Frontiers in Earth Science*, *6*, 197. https://doi.org/10.3389/feart.2018.00197

Musselman, K., Molotch, N., Margulis, S., Lehning, M., & Gustafsson, D. (2012). Improved snowmelt simulations with a canopy model forced with photo-derived direct beam canopy transmissivity. *Water Resources Research*, *48*, W10509. https://doi.org/10.1029/2012WR012285

Musselman, K. N., Molotch, N. P., & Brooks, P. D. (2008). Effects of vegetation on snow accumulation and ablation in a mid-latitude subalpine forest. *Hydrological Processes*, *22*, 2767–2776. https://doi.org/10.1002/hyp.7050

Musselman, K. N., Molotch, N. P., Margulis, S. A., Kirchner, P. B., & Bales, R. C. (2012). Influence of canopy structure and direct beam solar irradiance on snowmelt rates in a mixed conifer forest. *Agricultural and Forest Meteorology*, *161*, 46–56. https://doi.org/10.1016/j.agrformet.2012.03.011

Musselman, K. N., & Pomeroy, J. W. (2017). Estimation of needleleaf canopy and trunk temperatures and longwave contribution to melting snow. *Journal of Hydrometeorology*, *18*(2), 555–572. https://doi.org/10.1175/JHM-D-16-0111.1

Musselman, K. N., Pomeroy, J. W., & Link, T. E. (2015). Variability in shortwave irradiance caused by forest gaps: Measurements, modelling, and implications for snow energetics. *Agricultural and Forest Meteorology*, *207*, 69–82. https://doi.org/10.1016/j.agrformet.2015.03.014

Mutzner, R., Weijs, S., Tarolli, P., Calaf, M., Oldroyd, H., & Parlange, M. (2015). Controls on the diurnal streamflow cycles in two subbasins of an alpine headwater catchment. *Water Resources Research*, *51*, 3403–3418. https://doi.org/10.1002/2014WR016581

Nolin, A. (2010). Recent advances in remote sensing of seasonal snow. *Journal of Glaciology*, *56*(200), 1141–1150. https://doi.org/10.3189/002214311796406077

Painter, T. (2018). ASO L4 LiDAR snow depth 3m UTM grid, version 1. Grand Mesa Colorado. NASA National Snow and Ice Data Center Distributed Active Archive Center. Accessed November 2018. https://doi.org/10.5067/KIE9QNVG7HP0

Painter, T., Berisford, D. F., Boardman, J. W., Bormann, K. J., Deems, J. S., Gehrke, F., et al. (2016). The Airborne Snow Observatory: Fusion of scanning lidar, imaging spectrometer, and physically-based modeling for mapping snow water equivalent and snow albedo. *Remote Sensing of Environment*, *184*, 139–152. https://doi.org/10.1016/j.rse.2016.06.018

Pomeroy, J. W., Parviainen, J., Hedstrom, N., & Gray, D. M. (1998). Coupled modelling of forest snow interception and sublimation. *Hydrological Procedure*, *12*(15), 2317–2337. https://doi.org/10.1002/(SICI)1099-1085(199812)12:15<2317::AID-HYP799>3.0.CO;2-X

Raleigh, M., & Small, E. (2017). Snowpack density modeling is the primary source of uncertainty when mapping basin-wide SWE with lidar. *Geophysical Research Letters*, *44*, 3700–3709. https://doi.org/10.1002/2016GL071999

Revuelto, J., Lopez-Moreno, J., Azorin-Molina, C., & Vicente-Serrano, S. (2015). Canopy influence on snow depth distribution in a pine stand determined from terrestrial laser data. *Water Resources Research*, *51*, 3476–3489. https://doi.org/10.1002/2014WR016496

Roth, T., & Nolin, A. (2017). Forest impacts on snow accumulation and ablation across an elevation gradient in a temperate montane environment. *Hydrology and Earth System Sciences*, *21*(11), 5427–5442. https://doi.org/10.5194/hess-21-5427-2017

Rutter, N., Essery, R., Pomeroy, J., Altimir, N., Andreadis, K., Baker, I., et al. (2009). Evaluation of forest snow processes models (SnowMIP2). *Journal of Geophysical Research*, *114*, D06111. https://doi.org/10.1029/2008JD011063

Schneider, D., & Molotch, N. (2016). Real-time estimation of snow water equivalent in the Upper Colorado River Basin using MODIS-based SWE Reconstructions and SNOTEL data. *Water Resources Research*, *52*, 7892–7910. https://doi.org/10.1002/2016WR019067

Serreze, M. C., Clark, M. P., Armstrong, R. L., McGinnis, D. A., & Pulwarty, R. S. (1999). Characteristics of the western United States snowpack from snowpack telemetry (SNOTEL) data. *Water Resources Research*, *35*(7), 2145–2160. https://doi.org/10.1029/1999wr900090

Seyednasrollah, B., & Kumar, M. (2014). Net radiation in a snow-covered discontinuous forest gap for a range of gap sizes and topographic configurations. *Journal of Geophysical Research: Atmospheres*, *119*, 10,323–10,342. https://doi.org/10.1002/2014JD021809

Shah, R., Yueh, S., Xu, X., Chae, C.-S., Simard, M. & Elder, K. (2016). Snow water equivalent retrieval using P-band signals of opportunity, IEEE International Geoscience and Remote Sensing Symposium (IGARSS), 7064–7066.

Skiles, S. M. (2018). Grand Mesa study plot (version 1), Zenodo. https://doi.org/10.5281/zenodo.1479859

Sold, L., Huss, M., Hoelzle, M., Andereggen, H., Joerg, P., & Zemp, M. (2013). Methodological approaches to infer end-of-winter snow distribution on alpine glaciers. *Journal of Glaciology*, *59*(218), 1047–1059. https://doi.org/10.3189/2013JoG13J015

Sturm, M., Goldstein, M., & Parr, C. (2017). Water and life from snow: A trillion dollar science question. *Water Resources Research*, *53*, 3534–3544. https://doi.org/10.1002/2017WR020840

Sturm, M., & Holmgren, J. (2018). An automatic snow depth probe for field validation campaigns. *Water Resources Research*, *54*, 9695–9701. https://doi.org/10.1029/2018WR023559

Sun, N., Wigmosta, M., Zhou, T., Lundquist, J., Dickerson-Lange, S., & Cristea, N. (2018). Evaluating the functionality and streamflow impacts of explicitly modelling forest-snow interactions and canopy gaps in a distributed hydrologic model. *Hydrological Processes*, *32*(13), 2128–2140. https://doi.org/10.1002/hyp.13150

Tabler, R. D. (2003). Controlling blowing and drifting snow with snow fences and road design, NCHRP Project 20–7(147). National Cooperative Highway Research Program Transportation Research Board of the National Academies, (August), 346.

Tennant, C., Harpold, A., Lohse, K., Godsey, S., Crosby, B., Larsen, L., et al. (2017). Regional sensitivities of seasonal snowpack to elevation, aspect, and vegetation cover in western North America. *Water Resources Research*, *53*, 6,908–6,926. https://doi.org/10.1002/2016WR019374

Tinkham, W., Smith, A., Marshall, H., Link, T., Falkowski, M., & Winstral, A. (2014). Quantifying spatial distribution of snow depth errors from LiDAR using Random Forest. *Remote Sensing of Environment*, *141*, 105–115. https://doi.org/10.1016/j.rse.2013.10.021

Tischmacher, M., & Ruck, B. (2013). Interaction of gusts and forest edges an experimental wind-tunnel study. *Forestry*, *86*(5), 523–532. https://doi.org/10.1093/forestry/cpt029

Toms, J., & Lesperance, M. (2003). Piecewise regression: A tool for identifying ecological thresholds. *Ecology*, *84*(8), 2034–2041.

Troendle, C. A., & Meiman, J. R. (1986). The effect of patch clearcuttingg on the water balance of a subalpine forest slope. *Proceedings of the 54th Western Snow Conference* (pp. 93–100). Phoenix, AZ.

Troendle, C. A., Schmidt, R. A., & Martinez, M. H. (1988). Snow deposition processes in a forest stand with a clearing. *Proceedings of the 56th Western Snow Conference* (pp. 78–86). Kalispell, MO.

Trujillo, E., Ramirez, J., & Elder, K. (2007). Topographic, meteorologic, and canopy controls on the scaling characteristics of the spatial distribution of snow depth fields. *Water Resources Research*, *43*, W07409. https://doi.org/10.1029/2006WR005317

Trujillo, E., Ramirez, J., & Elder, K. (2009). Scaling properties and spatial organization of snow depth fields in sub-alpine forest and alpine tundra. *Hydrological Processes*, *23*(11), 1,575–1,590. https://doi.org/10.1002/hyp.7270

Vajda, A., Venalainen, A., Hanninen, P., & Sutinen, R. (2006). Effect of vegetation on snow cover at the northern timberline: A case study in Finnish Lapland. *Silva Fennica*, *40*(2), 195–207. https://doi.org/10.14214/sf.338

Varhola, A., & Coops, N. (2013). Estimation of watershed-level distributed forest structure metrics relevant to hydrologic modeling using LiDAR and Landsat. *Journal of Hydrology*, *487*, 70–86. https://doi.org/10.1016/j.jhydrol.2013.02.032

Varhola, A., Coops, N. C., Weiler, M., & Moore, R. D. (2010). Forest canopy effects on snow accumulation and ablation: An integrative review of empirical results. *Journal of Hydrology*, *392*(3–4), 219–233. https://doi.org/10.1016/j.jhydrol.2010.08.009

Webb, R. (2017). Using ground penetrating radar to assess the variability of snow water equivalent and melt in a mixed canopy forest, Northern Colorado. *Frontiers of Earth Science*, *11*(3), 482–495. https://doi.org/10.1007/s11707-017-0645-0

Webb, R. W., Fassnacht, S., & Gooseff, M. (2015). Wetting and drying variability of the shallow subsurface beneath a snowpack in California's Southern Sierra Nevada. *Vadose Zone Journal*, *14*(8). https://doi.org/10.2136/vzj2014.12.0182

Webb, R. W., Fassnacht, S. R., & Gooseff, M. N. (2018). Hydrologic flowpath development varies by aspect during spring snowmelt in complex subalpine terrain. *The Cryosphere*, *12*, 287–300. https://doi.org/10.5194/tc-12-287-2018

Webb, R. W., Jennings, K. S., Fend, M., & Molotch, N. P. (2018). Combining ground penetrating radar with terrestrial LiDAR scanning to estimate the spatial distribution of liquid water content in seasonal snowpacks. *Water Resources Research*, *54*, 10,339–10,349. https://doi.org/10.1029/2018WR022680

Webb, R. W., McGrath, D., Hale, K., & Molotch, N. P. (2018). SnowEx17 ground penetrating radar, version 1, NSIDC, Boulder, Colorado. https://doi.org/10.5067/NPZYNEEGQUO

Webb, R. W., Williams, M., & Erickson, T. (2018). The spatial and temporal variability of meltwater flowpaths: Insights from a grid of over 100 snow lysimeters. *Water Resources Research*, *54*, 1146–1160. https://doi.org/10.1002/2017WR020866

Webster, C., Rutter, N., Zahner, F., & Jonas, T. (2016). Measurement of incoming radiation below forest canopies: A comparison of different radiometer configurations. *Journal of Hydrometeorology*, *17*(3), 853–864. https://doi.org/10.1175/JHM-D-15-0125.1

Wheeler, K. (1987). Interception and redistribution of snow in a subalpine forest on a storm-by-storm basis. *Proceedings of the 55th Annual Western Snow Conference* (pp. 303–309). Vancouver, British Columbia.

Wilcoxon, F. (1945). Individual comparisons by ranking methods. *Biometrics*, *1*(6), 80–83.

Winstral, A., Elder, K., & Davis, R. E. (2002). Spatial snow modeling of wind-redistributed snow using terrain-based parameters. *Journal of Hydrometeorology*, *3*(5), 524–538. https://doi.org/10.1175/1525-7541(2002)003<0524:ssmowr>2.0.co;2

Woo, M. K., & Giesbrecht, M. A. (2000). Simulation of snowmelt in a subarctic spruce woodland: 1. Tree model. *Water Resources Research*, *36*(8), 2,275–2,285. https://doi.org/10.1029/2000WR900094